

Overview of Technologies for Millimeter-Wave OTA Measurements

Over The Air measurement will become important in the coming fifth-generation mobile communication technologies (5G) because of introduction of massive MIMO at micro-wave and millimeter-wave frequencies and requirements to mobile terminals for multiband and smaller size. The conventional Far-Field Measurement (FFM) method requires large-scale measurement infra-structure and long measurement time. In addition, using FFM in the millimeter-wave band suffers from low measurement accuracy caused by path loss due to the long transmission distance. We propose a Near-Field Measurement (NFM) method to solve these problems and help reduce measurement costs. Based on actual measurement results, this method offers improved measurement sensitivity and good match with FFM. We also introduce a NFM solution for the E-band using Non-Linear Transmission Line technology.

1 - Introduction

Radio equipment currently under development has yet to implement a measurement connector for the reasons out-lined below, making Over The Air (OTA) measurement technology of great importance.

First, there is the problem of the trend towards developing ever smaller mobile terminals and the need to cut parts costs. Current mobile-terminal designs have several built-in antennas supporting various wireless services, and the future rollout of 5G as well as the Internet of Things (IoT) will probably result in further increases in the antenna count. Implementing a measurement connector for each of these antennas would cause problems with mo-bile-terminal size and cost reduction trends.

Second, 5G base stations will use micro-wave and millimeter-wave Massive MIMO¹⁾ technologies. The increasing number of antenna connectors makes provision of a measurement connector for each antenna a practical impossibility.

Conventionally, the power and sensitivity of mobile terminals are measured using a measurement connector. At OTA measurement, the Total Radiated Power (TRP) and Total Isotropic Sensitivity (TIS)^{2),3)} of the mobile terminal are measured. Measurement of the antenna radiation pattern is a key evaluation item for Massive MIMO.

The basic OTA measurement method is the 3D integration method⁴⁾ using a radio anechoic chamber. In this method, the Equipment Under Test (EUT) surroundings are measured as a spheroid form. This method has problems with needing a radio anechoic chamber and large-scale measuring equipment. Moreover, since it uses far-field measurement (FFM), the electromagnetic wave loss due to free-space path loss in the millimeter-wave band is large, so there are problems with large measurement error and small measurement dynamic range. Other measurement methods using random field measurement^{5),6)} with a reverberation chamber, and a spheroidal coupler⁷⁾ have been proposed to solve these problems.

This paper examines Massive MIMO measurements. Massive MIMO is a technology using a very large number of antenna elements to support multi-user MIMO transmissions, and several antenna configurations supporting this technology have been proposed. For example, a configuration supporting control of all the antenna elements can create a digital-type antenna radiation pattern and another configuration using an analog phase shifter can control the beam directivity. The antennas used in Massive MIMO have very high directivity. Near-field measurement (NFM)^{(8),(9)} is a measurement method using these antenna types. In NFM, the far-field radiation pattern is calculated using the near-field electromagnetic field; NFM has low electromagnetic wave loss because measurement is performed near the antenna. Additionally, NFM not only measures the radiation pattern, but can also perform antenna diagnostics using the antenna near-field distribution.

First, this paper introduces planar NFM as a suitable method for performing Massive MIMO measurements. Next, it describes the measurement principle and some points to examine at actual measurement. We also introduce the Anritsu NFM measurement system. Finally, we propose an actual method for measuring Massive MIMO antennas.

2 - Near-Field Measurement (NFM)

2.1 NFM Measurement Principle

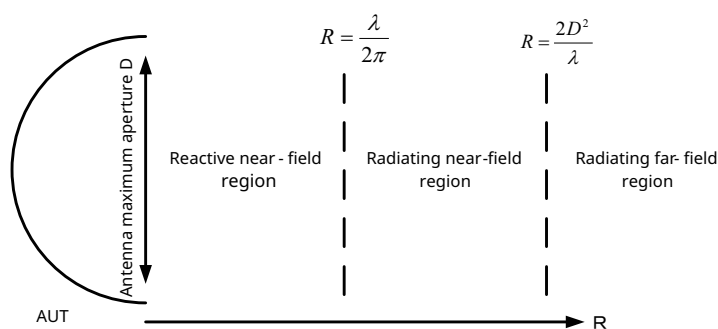


Figure 1: Antenna Measurement Regions

The electromagnetic field radiated from an antenna aperture is divided into regions as shown in Figure 1⁽¹⁰⁾. The region near the antenna aperture is called the reactive near-field region where most of the electromagnetic field components do not contribute to emission. The region where the radiation pattern does not change with distance from the antenna aperture is called the radiating far-field region. Generally, this is the region where the antenna radiation pattern is measured. The far field is defined as the distance R satisfying the following equation for the maximum diameter D of the antenna.

$$R = \frac{2D^2}{\lambda} \quad (1)$$

where, λ is the free-space wavelength. Additionally, the maximum power W_a received by the Rx antenna in free space is defined by the following equation where the Tx antenna gain is G_t , the Rx antenna gain is G_r , and the Tx power is W_t .

$$W_a = \left(\frac{\lambda}{4\pi R} \right)^2 G_t G_r W_t \quad (2)$$

Since a high-gain antenna with a larger aperture has larger R , the attenuation by free space becomes larger. The attenuation increases in the millimeter-wave band because λ is smaller and measurement of low-level side lobes becomes difficult.

The radiating near-field region (near-field) between these two regions is where the radiation pattern changes with distance. NFM measures the electromagnetic wave in the near field and finds the radiation pattern in the far field by calculation. The following explains the procedure for finding the radiation pattern in concrete terms. First, the region near the antenna is examined with a probe antenna connected to a Vector Network Analyzer (VNA) to determine the distribution of the electromagnetic field. Next, the radiation pattern at infinity is found by data processing the amplitude and phase of the captured electromagnetic field. The free space attenuation is small, because measurement is close to the antenna. Compared to far-field measurement, NFM can measure at higher accuracy. There are several types of NFM depending on the scanning area near the Antenna Under Test (AUT). This paper focuses on planar. This method is suitable for high-gain antennas and the data processing is simple. Figure 2 shows the relationship between the AUT and the scanning area. With planar NFM (NFM hereafter), a probe antenna is used to scan and measure the amplitude and phase of the electromagnetic field at a distance of the 3λ from the AUT. The distribution of the amplitude and phase at this measurement plane is the Fourier transformation of a function defined by the AUT radiation pattern and the probe antenna radiation pattern. Consequently, this function can be found by reverse Fourier transformation and the AUT radiation pattern can be found by filtering (probe correction) the probe antenna radiation pattern from the found function. The radiation pattern is calculated quickly by a computer because the data processing uses FFT.

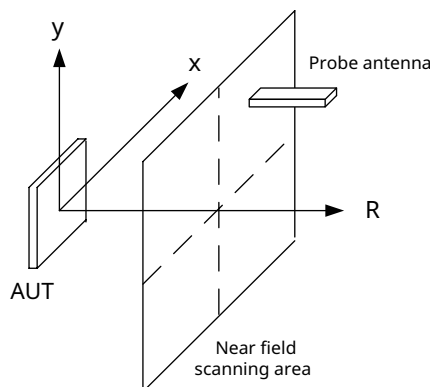


Figure 2: Planar NFM

2.2 Advantages of Near Field Measurement

Comparison of NFM and FFM		
Parameter	NFM	FFM
Measurement Location	Simple radio anechoic box	Radio anechoic chamber
Measurement Range	Near Field about 3λ (ex. 15 to 25 mm @ 60 GHz)	Far Field (ex. 3 m or 10m)
Radiation Pattern Measurement	3D	2D (3D radiation pattern measurement requires time and facilities)
Antenna Diagnostics and Analysis	Yes	Difficult

Table 1: Comparison of NFM and FFM

NFM has many advantages in comparison to FFM. Table 1 compares the two measurement methods. Since NFM is a close range measurement method, it does not require use of a radio anechoic chamber or other large scale facilities. The millimeter-wave measuring instruments are compact and the radiation pattern can be measured using a simple radio anechoic box in a room, which eliminates the problems of high cost and long time to configure a measurement system using a radio anechoic chamber. In addition, accurate measurement results are obtained because the method measures a region where the free space loss is small. In addition, NFM captures the entire radiation pattern (3D pattern) immediately in front of the AUT whereas FFM requires many measurements to capture the radiation pattern in two planes (2D radiation pattern)—the horizontal (H) plane, and the vertical (E) plane. Capturing the 3D radiation pattern using FFM requires a complex measurement setup and a longer measurement time. Additionally, NFM captures the amplitude and phase distribution near the antenna. If the radiation pattern cannot be captured due to the antenna design, the designer can use the captured amplitude and phase distribution to diagnose the cause. This point is of great benefit when measuring a phased-array antenna, such as a Massive MIMO antenna.

2.3 Scanning Area and Sampling Interval

The NFM scanning area is determined by the size of the AUT, the measurement frequency, and the required radiation pattern angular range. The scanning plane L_x when the measurement range of the required radiation pattern is θ_c as shown in Figure 3 is expressed by the following equation.

$$L_x = D + 2R \tan \theta_c \quad (3)$$

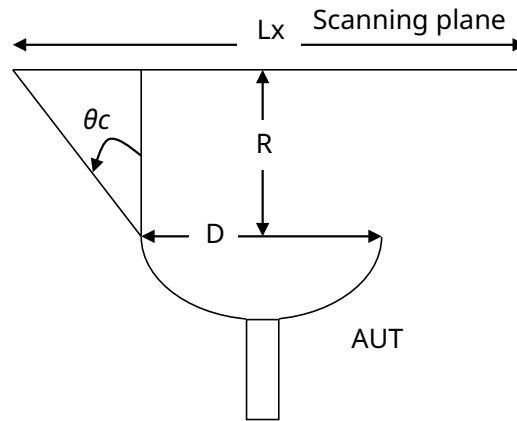


Figure 3: AUT Radiation Pattern and Scanning Field Relationship

For example, Table 2 shows the required scanning plane for 24 GHz and 60 GHz antennas. Assuming these are Massive MIMO antennas, each antenna is constructed of 8×8 parallel-aligned elements with a gap of 0.5λ .

AUT Parameters		
	AUT1	AUT2
Frequency [GHz]	24	60
Wavelength (λ) [mm]	12.5	5
Aperture (D) [mm]	57x57	23x23
Element distance [λ]	0.5	0.5
Number of elements	8x8	8x8
Directive gain [dBi]	24.2	24.2
Half-power beamwidth [deg.]	12.6	12.5

Table 2: AUT Parameters

If the antenna aperture distribution is assumed to be uniform, Table 2 shows the ideal gain and half-power beamwidth calculated from the aperture dimensions. The theoretical radiation pattern is shown in Figure 4. The measurement distance R is 4λ . The scanning plane of each antenna when $\theta_c = 60^\circ$ is expressed by Eq. 4 and Eq. 5.

$$AUT1: L_x = 57 + 2 \times 50 \tan 60[\text{deg.}] = 230 \text{ [mm]} \quad (4)$$

$$AUT2: L_x = 23 + 2 \times 20 \tan 60[\text{deg.}] = 92 \text{ [mm]} \quad (5)$$

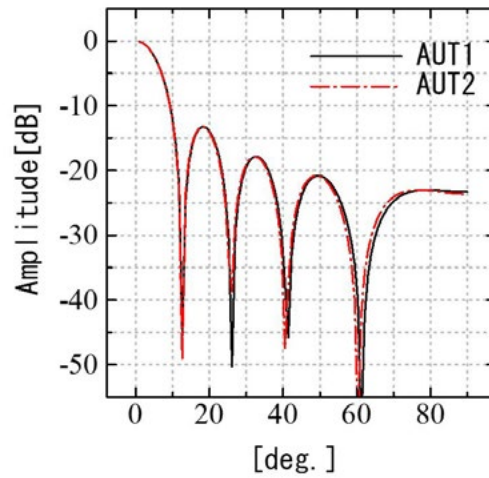


Figure 4: AUT Radiation Pattern Logical Values

Figure 4 shows that measurement up to the third side lobe is possible for AUT1 and AUT2. The scanning plane to measure up to the next side lobe is expressed by Eq. 6 and Eq. 7 where $\theta_c = 80^\circ$.

$$AUT1: L_x = 57 + 2 \times 50 \tan 80[\text{deg.}] = 624 \text{ [mm]} \quad (6)$$

$$AUT2: L_x = 23 + 2 \times 20 \tan 80[\text{deg.}] = 250 \text{ [mm]} \quad (7)$$

This result shows how the required scanning plane increases rapidly. To make the scanning plane small, the distance R should be small. However, multiple reflections occur between the probe antenna and the AUT and these reflections can impact the measurement results. From experience, the best distance between the probe and AUT is about 3 to 5 λ .

Next, we describe the sampling interval at near-field scanning. The sampling interval affects the radiation pattern angular range. When the sampling interval is wider, the angular range is narrower and vice versa. Since data outside the $\pm 90^\circ$ range is not required, a sampling interval of less than $\lambda/2$ is not required. Actually, the sampling interval is about 0.45 λ due to data processing issues.

2.4 Probe and Probe Correction

The probe antenna used for NFM requires the following three characteristics:

First, it must have the widest possible beamwidth. Ideally, an isotropic antenna should be used. However, the actual antenna has directivity. Consequently, the probe must be corrected. Probe correction removes the probe antenna radiation pattern from the AUT radiation pattern found by NFM. If a narrow-beam antenna is used as the probe antenna, the dynamic range of the radiation pattern is small and causes problems with accurate measurement of low-level side lobes.

Second, the cross-polarization ratio (XPR) must be small. The antenna radiation pattern is measured for each polarization. Linear polarization antennas are measured by splitting into vertical and horizontal polarizations, while circular polarization antennas are measured by splitting into right-hand circular and left-hand circular polarization. The polarization precision at NFM depends on the probe antenna polarization. To achieve precision measurements, it is necessary to use a probe antenna with the smallest possible XPR.

Third, multiple reflections between the probe antenna and AUT must be small. This issue can be resolved by using a small probe antenna covered by radio-wave absorber. To minimize the impact of multiple reflection on the measurement, research was done on a measurement method using an optical probe and optoelectric field conversion¹¹.

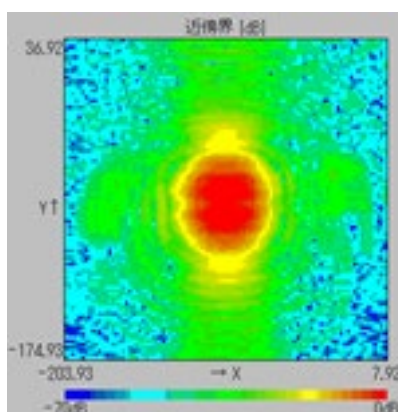
An open-ended waveguide is used as a probe antenna meeting the above described requirements in the millimeter-wave band. Since the aperture plane of this probe antenna is small, the beam is wide, the XPR is about -20 dB. Multiple reflections are suppressed by covering the probe antenna by radio-wave absorber.

2.5 Comparison of NFM and FFM Measurement Results

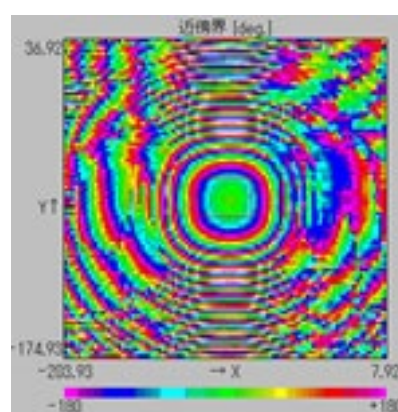
To confirm the appropriateness of NFM measurements, we compared the radiation pattern of the main polarization wave measured by NFM and FFM. A standard WR-15 horn antenna was used as the AUT, and Table 3 shows the NFM measurement parameters. FFM was performed using a radio anechoic chamber with six radio-wave absorbent surfaces. The distance between the AUT and Rx antenna was 5.1 meters.

NFM Measurement Parameters	
Frequency [GHz]	60.5
Sampling interval [mm]	2.23
Sampling number	96x96
Scanning area [mm]	211.85x211.85
Distance between AUT and probe [mm]	20

Table 3: NFM Measurement Parameters



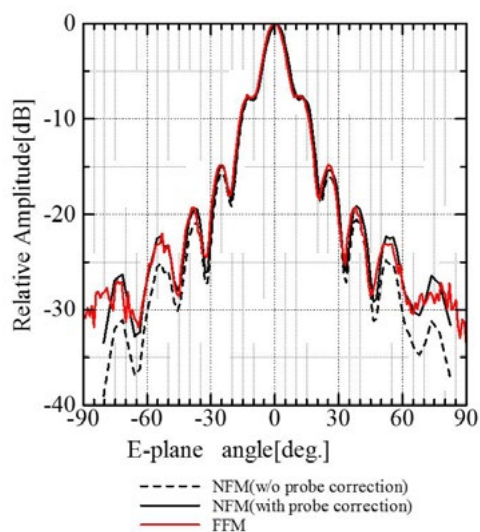
(a) Amplitude Distribution



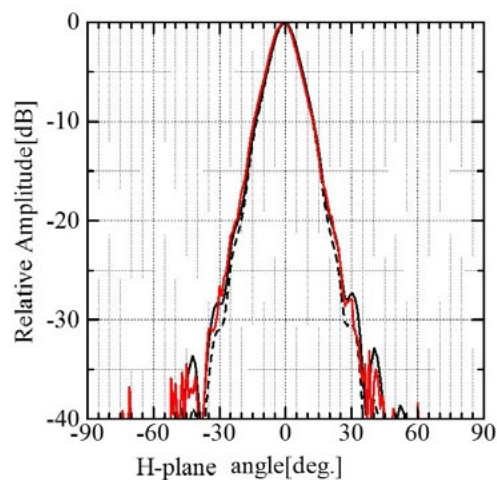
(b) Phase Distribution

Figure 5: Near-Field Scanning Results

Figure 5 shows the measured NFM distribution. Figure 6 shows the NFM and FFM radiation pattern results. From Figure 5 (a), there is clearly a region with a strong field at the center of the scanning plane. From Figure 5 (b), the same region in Figure 5 (a) with a strong field has an almost constant phase value. Based on this, the measurement results are a good match for the theoretical aperture distribution of a horn antenna. From Figure 6, the results for the corrected probe indicated by the solid black line are a better match with the FFM results indicated by the red line compared to the uncorrected probe results indicated by the dotted line. Additionally, Figure 6 (a) shows that the FFM results are affected by low-level noise of about -30 dB. However, this phenomenon could not be confirmed at NFM. These results confirm that probe correction is effective and NFM has better measurement sensitivity than FFM.



(a) Vertical Plane (E-plane) Radiation Pattern

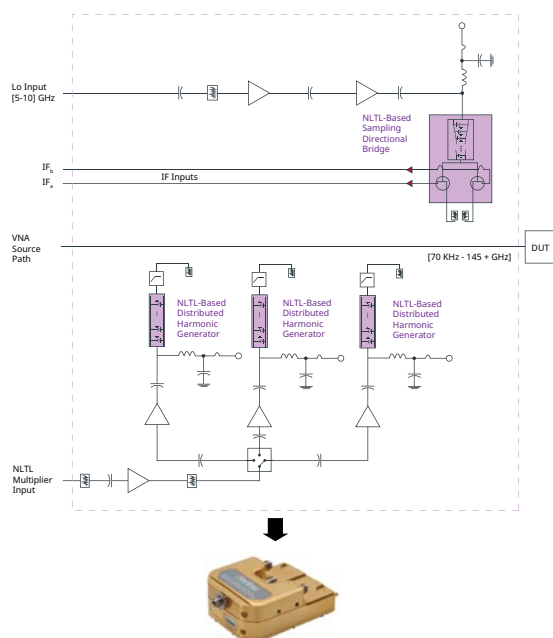


(b) Horizontal Plane (E-plane) Radiation Pattern

Figure 6: WR-15 Comparison of Standard Horn Antenna Radiation Patterns

3 - Anritsu NLTL Technology for Antenna Measurements

The insertion loss and phase stability of the coaxial cables in an antenna measurement setup such as that shown in Figure 8 deteriorate with frequency, thus reducing measurement accuracy and making antenna measurements in the millimeter-wave band and higher frequencies ever challenging. To deal with these challenges which are also common in millimeter-wave device testing, we recently introduced the world's first miniature commercial NLTL-based reflectometers and showed that these can be used to extend the frequency range of a microwave VNA to 145 GHz. Essential ingredients in this process are monolithic NLTL samplers used to extend the VNA receivers from 30 GHz to 145 GHz, NLTL harmonic generators used to extend the CW source from 54 GHz to 145 GHz, high directivity directional couplers, and a 0.8 mm coaxial port connector. The miniature 145 GHz reflectometer is shown in Figure 7 along



(a) 145 GHz NLTL VNA Frequency Extender



(b) 110 GHz NLTL VNA Frequency Extender

with a previous version limited to 110 GHz.

Figure 7: VNA reflectometers for extending the frequency range of a 70 GHz VNA to (a) 145 GHz (b) 110 GHz

In addition to their miniature size, these reflectometers provide highly attractive features such as short/long term thermal stability due to the vanishing thermal gradient across the modules, high amplitude and phase stability, and raw directivity to mention a few. Most importantly, placing the sampling directional bridge closest to the AUT/DUT provides long term amplitude and phase stability. It is these features in particular that lend themselves well to antenna measurements whether these are performed in a near field, far field, or compact range scenario. In order to reduce the cable complexity and address opportunities in high-frequency 5G communications where multi-port measurements are required, we introduced an E-band version of the reflectometers based on a modular AXIe format as shown in Figure 8.

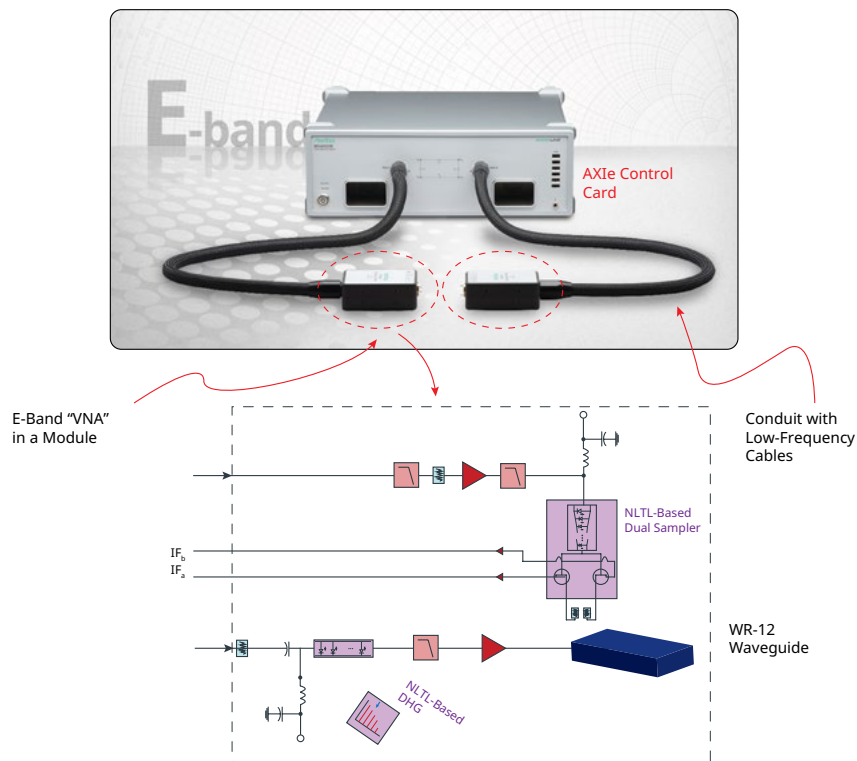


Figure 8: E-band VNA driven by an AXIe modular card

The E-band modules retain the benefits of their broadband counterparts and provide port scalability as a result of the modular nature of the driver cards. In addition, the conduits used to reduce the cable complexity provide a framework for extending the length of the cables for far-field antenna measurements. A near-field antenna measurement setup based on these reflectometers is shown in Figure 9.

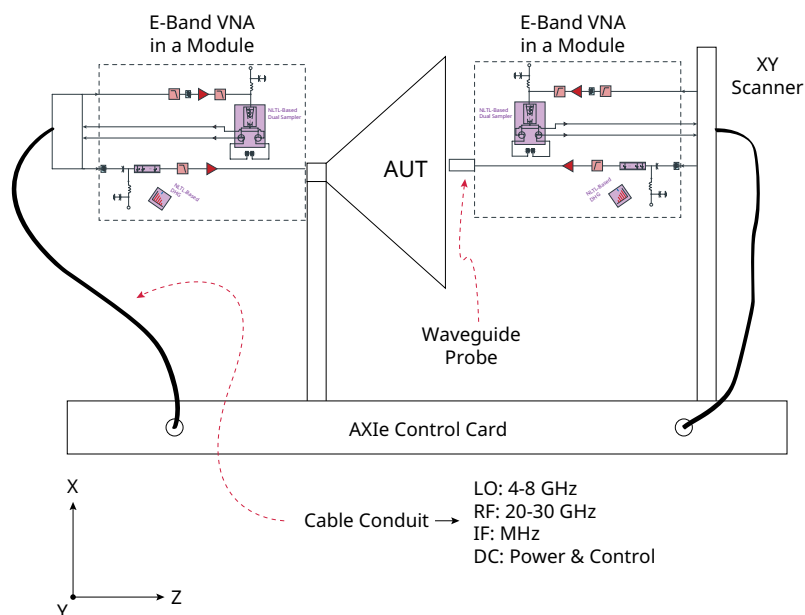


Figure 9: Nearfield E-band antenna measurement setup. The reflectometers are brought closest to the antenna ports.

It is evident in Figure 9 that by bringing the reflectometers closest to the waveguide probe on one hand and the AUT on the other, mm-wave coaxial cable losses are eliminated when compared with a traditional measurement setup. Phase and magnitude stability are also improved as is shown in Figure 10 over an 8 hour period.

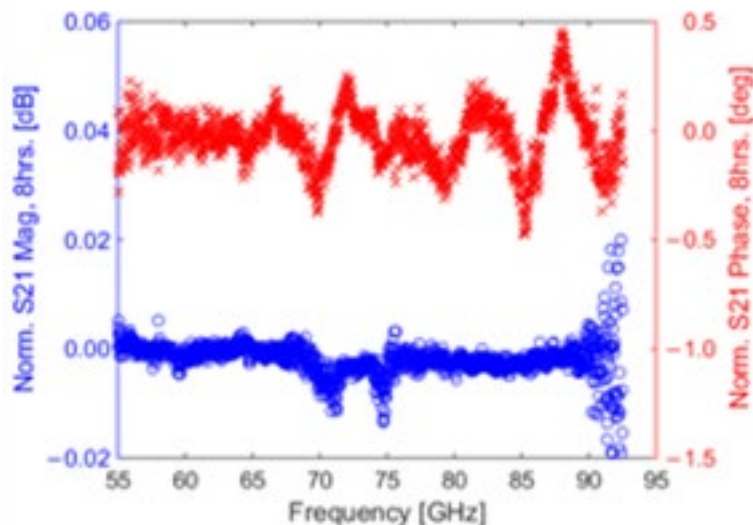


Figure 10: Measured magnitude and phase variation over a period of 8 hours.

4 - Massive MIMO Antenna Measurement System

A general-purpose antenna commonly has a beam direction at right angles to the antenna front as shown in Figure 11 (a). The Massive MIMO antenna proposal changes the antenna radiation direction as shown in Figure 11 (b) by changing the phase of the antenna elements. The following two problems can be assumed when performing NFM using an antenna with a radiation pattern like that shown in Figure 11 (b).

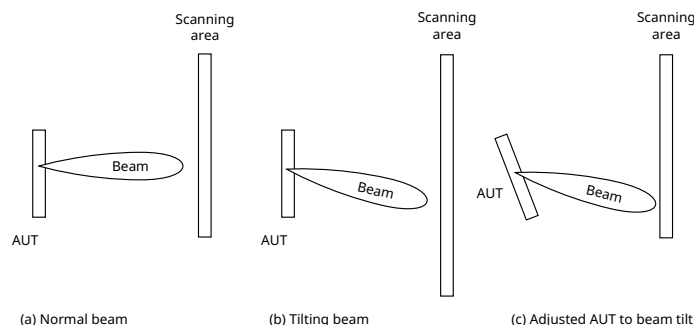


Figure 11: AUT Beam Direction and Near Field Scanning Area

First, the near-field scanning area is enlarged. As described in section 2.3 above, with NFM when the required radiation pattern measurement area is wider, the required near-field scanning area becomes larger. As a result, when the AUT beam is tilted as shown in Figure 11 (b), finding the radiation pattern of the wide angle matching this tilt re-quires a wide scanning area.

Second, the measurement accuracy becomes worse. FFT is used to calculate the radiation pattern from the near-field distribution. The calculated AUT radiation pattern interval is narrowest near the center (E-plane 0° , H-plane 0°) based on a feature of this calculation. Conversely, the interval of the radiation pattern calculation point becomes wider as the angle becomes larger. As a result, the beam is not near the center so the measurement accuracy may become worse when the beam width is narrow.

To solve these problems when using NFM to measure a Massive MIMO antenna, we propose the measurement system shown in Figure 12. This system is composed of an XY positioner for scanning the near field and Az and El tables attached to the AUT. Using this design, the measurement system can perform measurement even when the AUT beam direction changes. Figure 13 lists the actual measurement steps. In the case of AUT arrangement in Figure 11 (b), 1-line scans in horizontal and vertical plane are per-formed to obtain beam direction. Using this result, the AUT direction is controlled by the Az and El tables and the AUT beam center is matched with the center of the near-field scanning area as shown in Figure 11 (c). Using this arrangement, the AUT beam is always at the center of the calculated radiation pattern (E-plane 0° , H-plane 0°), which minimizes the measurement area and suppresses any de-graded accuracy. Moreover, if the AUT phase shifter can be operated from the same system, the radiation pattern can be measured automatically while the beam direction changes. We expect to be able to shorten AUT measurement times in this way.

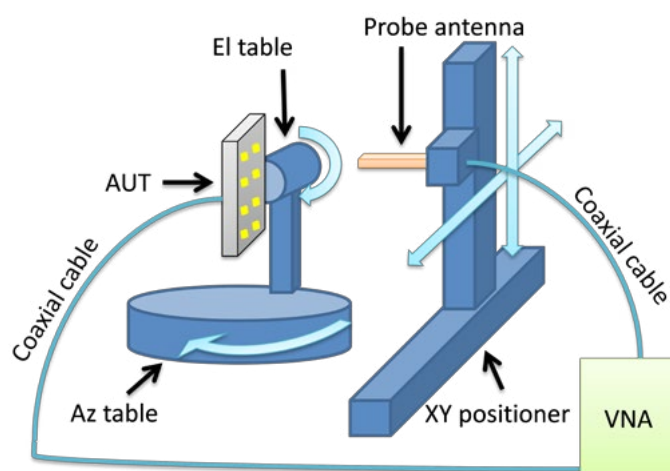


Figure 12: Massive-MIMO Measurement NFM

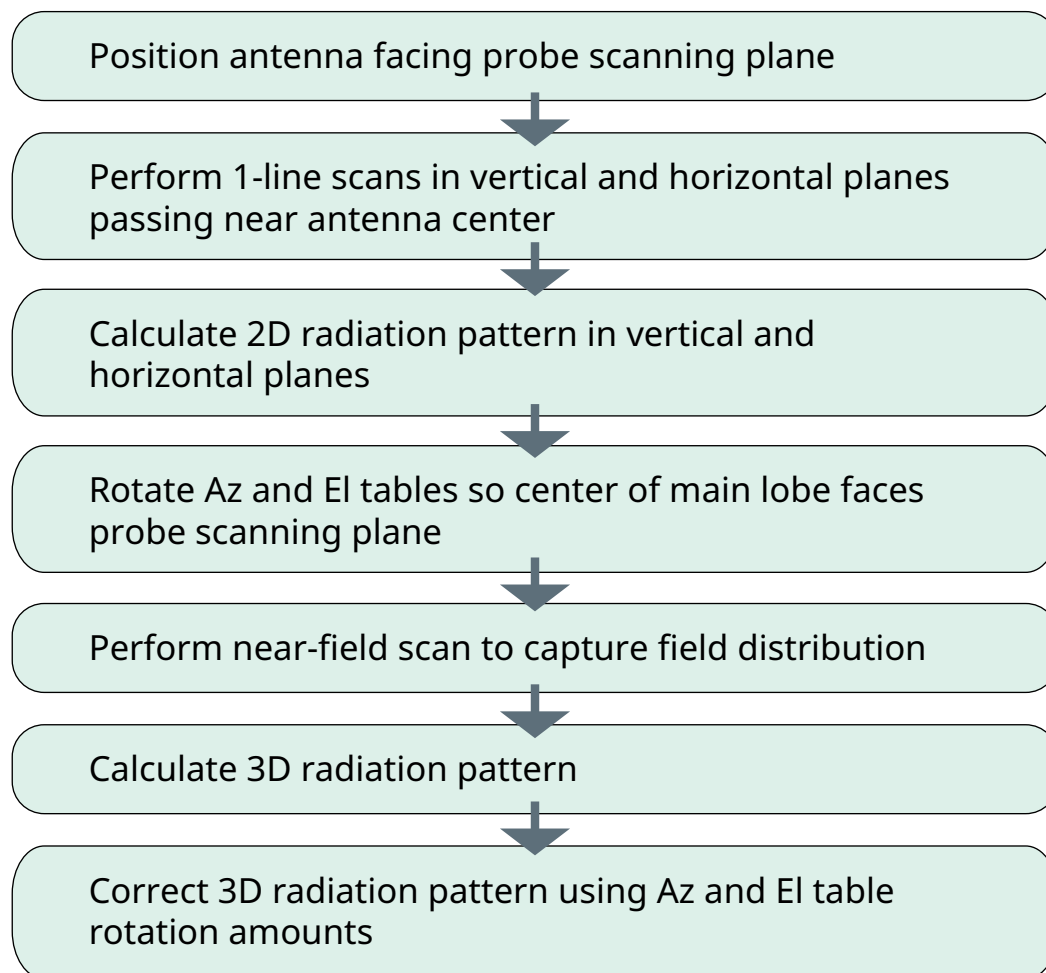


Figure 13: Measurement Flowchart

5 - Conclusions

This paper proposes NFM as a system for measuring Massive MIMO antennas. It describes the basic principles of NFM and presents some measurement results indicating good agreement between NFM and FFM measurements. The NFM method reduces free-space losses, supporting measurement with good sensitivity. This system is shown to be suitable for OTA measurements in the micro-wave and millimeter-wave bands. Additionally, we introduce our NFM system supporting E-band measurements and propose an NFM system solving the problems of measuring Massive MIMO antennas. Future work is examining designs for solving issues with OTA measurements under actual usage conditions, which we hope will help speed development of 5G and millimeter-wave communications.

6 - References

- T. Nakamura, A. Benjebbour, Y. Kishiyama, S. Suyama, T. Imai, "5G Radio Access: Requirements, Concept and Experimental Trials", IEICE Trans. Commun., vol. E98-B, no. 8, pp. 1397-1406, (2015-8)
- Cellular Telecommunications & Internet Association, Test Plan for Mobile Station Over the Air Performance; Method of Measurement for Radiated RE Power and Receiver Performance, Revision 2.1, (2005-4)
- 3GPP TS 34.114 V9.1.0 (2011-03) 3rd General Partnership Project; Technical Specification Group Radio Access Net-work; User Equipment (UE)/Mobile Station (MS) Over The Air (OTA) antenna performances; Conformance testing (Release 9)
- IEC60498-1, "Amendment 2 Methods of measurement for radio equipment used in the mobile services - Part 1: General definitions and standard conditions of measurement"
- K. Harima, "Statistical Characteristics of E-Field Distribution in a Reverberation Chamber", IEICE Trans. Commun., vol. E88-B, no. 8, pp. 3127-3132, (2005-8)
- T. Sugiyama, T. Shinozuka, K. Iwasaki, "Estimation of radiated power of radio transmitters using a reverberation chamber", IEICE Trans. Commun., vol. E88-B, no. 8, pp. 3158-3163, (2005-8)
- T. Teshirogi, T. Kawamura, A. Yamamoto, T. Sakuma, Y. Nago, S. Mattori, "Over-The-Air Measurements of Small Radio Terminals using Spheroidal Coupler", IEICE Trans. Commun., vol. E95-B, no. 6, pp. 2043-2050, (2012-6)
- D. M. Kerns, "Plane-wave scattering matrix theory of antennas and antenna-antenna interactions: formulation and applications", NBS Monograph 162, (1981-6)
- D. Slater: Near-field antenna measurements, Artech House Publishers, Norwood. MA, USA, (1991)
- Y. T. Lo, S. W. Lee: Antenna Handbook, Vol.1, Chapman & Hall, New York, NY, USA, (1993)
- M. Hirose, T. Ishizone, K. Komiyama, "Antenna Pattern Measurements Using Photonic Sensor for Planar Near-Field Measurement at X Band", IEICE Trans. Commun., vol. E87-B, no. 3, pp. 727-734, (2004-3)

7 - Authors

Takashi Kawamura

Technical Headquarters
Advanced Technology
Development Center

Hanako Noda

Technical Headquarters
Advanced Technology
Development and
Planning Center

Karam Noujeim

Technology Fellow
Director Network
Infrastructure Business
Unit (NIBU) - Americas

Publicly available